Electronic reconstruction and interface engineering of emergent spin fluctuations in compressively strained La₃Ni₂O₇ on SrLaAlO₄(001)

Benjamin Geisler, ^{1,2,*} James J. Hamlin, ¹ Gregory R. Stewart, ¹ Richard G. Hennig, ^{2,3} and P.J. Hirschfeld ¹

¹Department of Physics, University of Florida, Gainesville, Florida 32611, USA
²Department of Materials Science and Engineering, University of Florida, Gainesville, Florida 32611, USA
³Quantum Theory Project, University of Florida, Gainesville, Florida 32611, USA
(Dated: March 17, 2025)

Motivated by the recent observation of ambient-pressure superconductivity with $T_c \sim 40$ K in La $_3$ Ni $_2$ O $_7$ on SrLaAlO $_4$ (001), we explore the structural and electronic properties as well as the spin-spin correlation function of this bilayer nickelate system by using density functional theory including a Coulomb repulsion term. We find that the compressive strain exerted by this substrate leads to an unconventional occupation of the antibonding Ni $3d_{z^2}$ states, distinct from the superconducting bulk compound under pressure. While pure strain effects rather modestly enhance the dynamical spin susceptibility via Fermi surface nesting, investigation of a reconstructed interface composition as observed in transmission electron microscopy uncovers a strong amplification of the spin fluctuations. These results provide insights into the emergence of superconductivity in strained La $_3$ Ni $_2$ O $_7$, suggest a possible key role of the interface, and highlight fundamental differences from the hydrostatic pressure scenario

I. INTRODUCTION

The discovery of superconductivity with $T_c \sim 80$ K in pressurized La₃Ni₂O₇ [1–3] has identified bilayer Ruddlesden-Popper nickelates as a fascinating new addition to the growing family of superconducting nickelates. This breakthrough has sparked significant theoretical and experimental interest [4–39]. Unlike infinite-layer nickelates, where superconductivity is limited so far to thin films [40–48], La₃Ni₂O₇ exhibits superconductivity in bulk crystals. The pairing mechanism has been linked to a pressure-driven Fermi surface reconstruction [1, 4–6, 16] and an associated orthorhombic-totetragonal structural transition [24, 30], which suppresses octahedral rotations [1, 16, 24, 30]. Depending on the balance of the involved Ni 3d orbitals, it may correspond to d-wave or s^{\pm} symmetry [7, 16, 21, 49].

Recently, epitaxial strain has been proposed by density functional theory as a promising route to induce ambient-pressure superconductivity in La₃Ni₂O₇ [50–52]. Enhanced spin fluctuations have been predicted particularly for tensile strain in La₃Ni₂O₇/SrTiO₃(001) [50]. Intriguingly, independent experiments have since reported the observation of ambient-pressure superconductivity with a transition onset of up to $T_c \sim 40$ K in capped bilayer nickelate thin films of 4 to 6 bilayers grown on SrLaAlO₄(001) (SLAO) [53–55], after previous attempts did not detect a superconducting transition for compressive or tensile strain [56]. This necessitates the identification of potential differences to the physics of bilayer nickelates under high pressure and how they relate to the pairing mechanism.

Here we explore the structural and electronic properties of La₃Ni₂O₇/SrLaAlO₄(001) by using density functional theory including a Coulomb repulsion term, with an explicit treatment of the interface. In addition to the ideal interface stacking, we consider a reconstructed interface composition

that has recently been identified in transmission electron microscopy (TEM) [53]. Structural analysis reveals close agreement with recent x-ray diffraction (XRD) and TEM data for La₃Ni₂O₇ on different prominent substrates [57] and emphasizes the importance of the interfacial reconstruction. We observe finite octahedral tilts throughout the bilayer nickelate, which surprisingly are quenched at the reconstructed interface due to geometric constraints. We find that compressive strain in the presence of a substrate induces an electronic reconstruction in La₃Ni₂O₇, characterized by an unconventional partial occupation of the antibonding Ni $3d_{z^2}$ states. Interestingly, while strain alone leads to a rather modest enhancement of the dynamical spin susceptibility as a result of Fermi surface nesting, the reconstructed interface composition substantially amplifies the spin fluctuations. A detailed disentanglement of the scattering channels reveals that the amplified fluctuations are driven by the emergent interfacial Ni $3d_{z^2}$ states.

These results suggest that the enhanced pairing in compressively strained La₃Ni₂O₇ arises from a different set of electronic excitations than the flat-band driven superconductivity in the bulk compound under hydrostatic pressure. The pronounced sensitivity to the interface geometry highlights the potential of interface engineering in shaping the electronic properties and spin fluctuations in bilayer nickelates, opening new avenues for manipulating their superconducting phase.

II. RESULTS

A. Interface geometry and electronic reconstruction in La₃Ni₂O₇/SrLaAlO₄(001)

Figure 1 shows the optimized geometry and layer-resolved density of states of epitaxial La₃Ni₂O₇ on SLAO(001). We descibe the system by using symmetric $\sqrt{2}a \times \sqrt{2}a \times c$ supercells that contain two equivalent interfaces (see Methods). The substrate features a lattice constant of $a_{\rm SLAO}=3.756$ Å [53, 57] and exerts $\varepsilon=a_{\rm SLAO}/a_{\rm LNO}-1\approx-1.9\%$ compressive strain on the bilayer nickelate, which has a pseu-

^{*} benjamin.geisler@ufl.edu

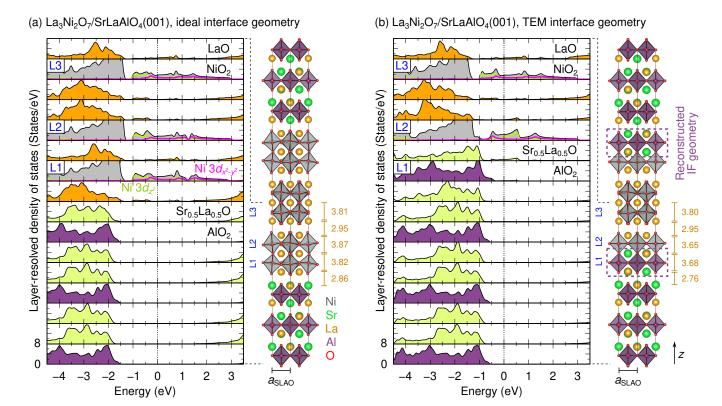


Figure 1. **Optimized geometry and layer-resolved density of states of La₃Ni₂O₇/SrLaAlO₄(001).** (a) Ideal interface stacking, representing a natural continuation of the two constituent oxides. (b) Interface composition as observed in recent TEM experiments [53], consisting of an Al_{Ni} substitution in layer L1 and a mixed $Sr_{0.5}La_{0.5}$ configuration at the adjacent A sites (purple dashed rectangles). The orange numbers denote the A-site distances in z direction. Both systems show no involvement of the substrate in the Fermi surface, although the interface reconstruction significancy reduces the energy difference between the Fermi level and the valence band maximum of the substrate.

docubic lattice parameter of $a_{\rm LNO}=3.83$ Å. We compare two representative interface geometries: the ideal interface, which represents a natural continuation of the two constituent structures [Fig. 1(a)], and a reconstructed geometry as suggested by recent TEM imaging [53]. The latter consists in substituting Al for Ni ions in layer L1, while the adjacent A sites adopt a mixed $Sr_{0.5}La_{0.5}$ configuration instead of pure La ions, which we treat explicitly here [Fig. 1(b)].

For the ideal interface geometry [Fig. 1(a)], the vertical A-site distances in the nickelate are enhanced to 3.82-3.87 Å due to compressive strain, compared to the bulk value of 3.70 Å, and exhibit only minor variations. In contrast, for the reconstructed interface [Fig. 1(b)], the A-site distance across layer L2 is notably reduced to 3.65 Å due to the proximity of the AlO $_2$ layer L1. We observe an expansion of the bilayer separation to 2.95 Å in both systems, relative to the bulk value of 2.90 Å.

We identify finite octahedral tilts throughout the nickelate region in both optimized geometries (Fig. 1). This contrasts with their assumed suppression in superconducting bulk $La_3Ni_2O_7$ under high pressure [1, 16, 24, 30]. Interestingly, a notable exception occurs in layer L2 near the reconstructed interface, where the NiO_6 octahedral tilts are quenched. This phenomenon is likely driven by the direct connectivity to the

rigid, untilted AlO₆ octahedra in layer L1, which impose a geometric constraint on the adjacent nickelate layer.

Along the [001] direction, each bilayer of the 327 Ruddlesden-Popper nickelate consists of three $(\text{LaO})^{1+}$ and two $(\text{NiO}_2)^{1.5-}$ layers, yielding a nominal Ni $3d^{7.5}$ valence. The SLAO substrate, on the other hand, is a band insulator with a formal Al^{3+} valence state and adopts a 214 Ruddlesden-Popper structure, consisting of single $(\text{AlO}_2)^{1-}$ layers confined in two $(\text{Sr}_{0.5}\text{La}_{0.5}\text{O})^{0.5+}$ layers. At the ideal interface, the nickelate-substrate separation amounts to 2.86 Å, while it is contracted to 2.76 Å at the reconstructed interface (Fig. 1). This reduction can be directly attributed to the lowered formal polarity of the AO layers involved. For reference, $\text{La}_3\text{Ni}_2\text{O}_7$ on non-polar SrTiO $_3(001)$ presents a similar interfacial A-site distance of 2.78 Å [50].

The layer-resolved densities of states in Fig. 1 show the relative band alignment of the constituent oxides. We find in both systems that the Fermi energy is clearly located in the substrate band gap. Therefore, the Fermi surfaces shown in Fig. 2(d) are exclusively formed by the Ni e_g states. The interface reconstruction reduces the energy difference between the Fermi level and the valence band maximum of the substrate from ~ 1.5 to ~ 0.6 eV. In contrast to La₃Ni₂O₇/LaAlO₃(001), where the polar discontinuity at the

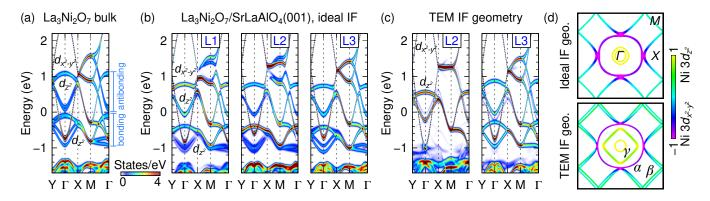


Figure 2. Electronic structure of the strained bilayer nickelate systems. Momentum-resolved density of states, projected on the Ni 3d orbitals (b) in layers L1-L3 of La₃Ni₂O₇/SLAO(001) with ideal interface and (c) in layers L2-L3 of La₃Ni₂O₇/SLAO(001) with reconstructed interface (cf. Fig. 1). Consistently obtained Ni 3d bands for bulk La₃Ni₂O₇ at ambient pressure are shown for comparison in panel (a). In the reconstructed system, Ni is substituted by Al in layer L1; hence, the adjacent layer L2 presents a single Ni $3d_{z^2}$ band instead of a bonding-antibonding pair. (d) Fermi surfaces, colored by the Ni orbital character $(3d_{z^2} - 3d_{x^2-y^2})/(3d_{z^2} + 3d_{x^2-y^2})$. Intriguingly, compressive strain leads to the occupation of the *antibonding* Ni $3d_{z^2}$ states at the Γ point (γ electron pockets), in sharp contrast to the flat-band physics arising in pressurized bulk La₃Ni₂O₇.

interface leads to an electron doping of the nickelate superconductor [50], we do not observe interfacial charge transfer for the present systems.

Figure 2 shows the projected momentum-resolved density of states, $A_i(\epsilon, k) = \sum_n \langle \phi_i | \psi_{n,k} \rangle \, \delta(\epsilon_{n,k} - \epsilon)$, where ϕ_i denotes Ni 3d manifolds at different sites i. In general, compressive strain drives a significant charge transfer from the Ni $3d_{x^2-y^2}$ reservoir to the Ni $3d_{z^2}$ states, since the concomitant vertical expansion of the nickelate region tends to lower the energy of the Ni $3d_{z^2}$ orbital relative to Ni $3d_{x^2-y^2}$. Intriguingly, this allows to control the Ni e_g orbital polarization $(3d_{z^2}-3d_{x^2-y^2})/(3d_{z^2}+3d_{x^2-y^2})$ over a considerably larger interval than hydrostatic pressure [50]. Here, we find that this mechanism leads to an unconventional occupation of the antibonding Ni $3d_{z^2}$ states around the Γ point [Fig 2(b)], which are empty in the bulk [Fig 2(a)], even at finite pressure. Their occupation is fairly uniform among the different layers, signaling the absence of electrostatic doping. Simultaneously, the bonding Ni $3d_{z^2}$ states are entirely filled and their flatband-like maximum is lowered to ~ -0.4 eV in all layers.

Importantly, this picture applies to the system with reconstructed interface as well [Fig 2(c)]. Due to the Al_{Ni} substitution in layer L1, the adjacent layer L2 presents a single Ni $3d_{z^2}$ band instead of a bonding-antibonding pair [Fig 2(c)]. It is more strongly filled than the other Ni $3d_{z^2}$ bands in either the ideal or the reconstructed system and provides a substantial contribution to the total density of states at the Fermi energy [Fig. 1(b)], which plays a central role in the spin susceptibility enhancement (see below). Analysis of the layer polarities leaves the NiO₂ layer L2 in a formal 1- state, leading to an altered local Ni³⁺ valence similar to bulk LaNiO₃. Interestingly, this interfacial NiO₂ layer is embedded in a highly anisotropic chemical environment, which induces a considerable Ni e_q orbital polarization. This effect is even more pronounced than in LaNiO₃/LaAlO₃(001) superlattices, which have been widely explored in the context of Fermi surface engineering and nickelate superconductivity [58, 59].

The Fermi surface of La₃Ni₂O₇ is known to consist of two characteristic sheets: an α sheet of predominantly Ni $3d_{x^2-y^2}$ character and a β sheet with some admixture of Ni $3d_{z^2}$ [4– 6, 27]. Under hydrostatic pressure [1, 4–7, 16, 21] or tensile strain as imposed by SrTiO₃(001) [50], the system undergoes a topological transition, leading to the emergence of a hole pocket due to a metallization of the bonding Ni $3d_{z^2}$ states. In stark contrast, our simulations for compressively strained La₃Ni₂O₇/SLAO(001) reveal a distinct Fermi surface composition, reflecting the differences in electronic reconstruction [Fig. 2(d)]. The β sheet exhibits an enhanced Ni $3d_{z^2}$ contribution compared to the bulk, while the α sheet appears more rectangular and features a significantly promoted Ni $3d_{x^2-y^2}$ character. Additional electron pockets emerge near the Γ point, originating from the partial occupation of the antibonding Ni $3d_{z^2}$ states (γ). For the reconstructed interface composition, we find a notable splitting of the β sheet. Moreover, a larger electron pocket around the Γ point can be observed, predominantly associated with Ni $3d_{z^2}$ states localized in layer L2, and a smaller pocket that stems from layer L3 [Fig. 2(c,d)]. These results highlight the effect of interface reconstructions on the electronic structure and suggest their critical role in the modulation of the superconducting properties. We will corroborate this aspect by calculating the dynamical spin susceptibility below.

B. Structural properties of bilayer nickelates on different substrates

The availability of high-quality x-ray diffraction and TEM data on strained epitaxial thin films [57], specifically for the evolution of the vertical lattice parameter of the bilayer nickelate, offers a unique opportunity to systematically compare experimental observations with the optimized structures re-

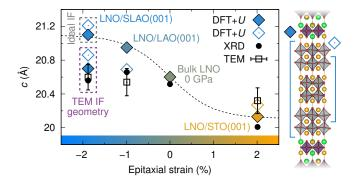


Figure 3. Structural properties of bilayer nickelates on different substrates. Evolution of the effective $c_{\rm LNO}$ of La₃Ni₂O₇ (LNO) as a function of the epitaxial strain ε . For the DFT+U-optimized structures reported here and in previous work [50], we show $c_{\rm LNO}$ measured in two different ways as described in the text (filled and empty diamonds; see structure on the right). The results are compared to recent XRD and TEM measurements for strained La₃Ni₂O₇ thin films [57] and XRD for bulk LNO at ambient pressure [60].

ported here and in previous work [50]. Extracting an effective nickelate lattice parameter $c_{\rm LNO}$ from the optimized structures can be performed in different ways, which yield slightly different values. In Fig. 3, we present $c_{\rm LNO}$ obtained by using two distinct methods: (i) The *outer* distance (filled diamonds) is defined as the distance between the two interfaces. This corresponds to $3/2 \cdot c_{\rm LNO}$ of an orthorhombic La₃Ni₂O₇ reference cell. (ii) The *inner* distance (empty diamonds) corresponds to $2/2 \cdot c_{\rm LNO}$ and captures more specifically the internal structural response of the nickelate layer.

Interestingly, we find that the outer distance follows approximately a $tanh(\varepsilon)$ function (dashed black line), a behavior observed also in LaNiO₃/LaAlO₃(001) superlattices [61]. For La₃Ni₂O₇/SLAO(001), it yields $c_{LNO} = 21.10 \text{ Å}$ (ideal interface) and 20.70 Å (reconstructed interface). Both values clearly exceed the bulk reference of 20.6 Å [24], indicating a significant strain-induced vertical expansion of the nickelate. The inner distance, which generally renders slightly larger values, yields $c_{LNO} = 21.21 \text{ Å}$ (ideal interface) and 20.86 Å (reconstructed interface). We observe that the reconstructed interface geometry reduces c_{LNO} considerably, bringing the theoretical predictions for La₃Ni₂O₇/SLAO(001) into close agreement with the experimental TEM and XRD results (Fig. 3). For La₃Ni₂O₇/SrTiO₃(001) (LNO/STO), we obtain very good agreement between theoretical and experimental values as well. For La₃Ni₂O₇/LaAlO₃(001) (LNO/LAO), the inner distance aligns closely with the experimental data, whereas the outer distance is notably higher, reflecting the complex interplay of interfacial charge transfer and structural distortions in this system.

Overall, our DFT+U predictions agree within a $\pm 0.8\%$ margin with the experimental lattice constants over a wide range of strain values ε from -2% to 2%, despite systematic uncertainties in the theoretical and experimental data. This comparison underscores the impact of interface effects on the structural parameters. The values compiled in Fig. 3 will be a

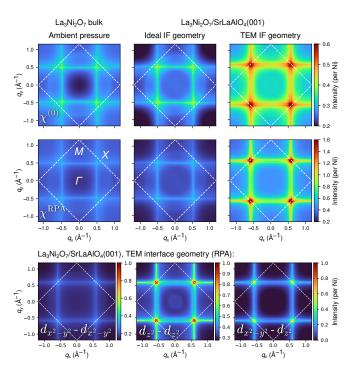


Figure 4. Spin-spin correlation functions $\chi^{(0)}(\mathbf{q})$ and $\chi^{\text{RPA}}(\mathbf{q})$. The results have been unfolded from the $\sqrt{2}\times\sqrt{2}$ (dashed lines) to the full Brillouin zone. An enhanced magnitude and sharpness of the peaks along the (π,π) direction can be observed in the strained systems with respect to bulk La₃Ni₂O₇ at ambient pressure, particularly in the case of the experimentally observed interface reconstruction. The orbital-resolved scattering contributions to $\chi^{\text{RPA}}(\mathbf{q})$ for La₃Ni₂O₇/SLAO(001) with reconstructed interface (bottom row) are largest for the intraorbital $3d_{z^2}$ and interorbital $3d_{x^2-y^2}$ - $3d_{z^2}$ channels.

helpful reference for future experimental studies.

C. Spin susceptibility in La₃Ni₂O₇/SrLaAlO₄(001)

The superconducting pairing is determined by the dynamical spin susceptibility $\chi^{\text{RPA}}(\mathbf{q})$, which we compare in Fig. 4 considering a Kanamori-type interaction vertex with U=0.6 and J=0.2 eV in the random phase approximation (RPA). For completeness, we also show the bare Lindhard susceptibility $\chi^{(0)}(\mathbf{q})$.

The spin susceptibility of bulk La₃Ni₂O₇ at ambient pressure is dominated by intraorbital $3d_{x^2-y^2}$ scattering [50]. Direct comparison reveals that La₃Ni₂O₇/SLAO(001) exhibits a moderately enhanced magnitude and sharpness of the characteristic susceptibility peaks along the (π,π) direction. The difference can be traced back to the intraorbital $3d_{z^2}$ and interorbital $3d_{x^2-y^2}$ - $3d_{z^2}$ channels (not shown).

Intriguingly, we find a very strong enhancement of the susceptibility for the $\text{La}_3\text{Ni}_2\text{O}_7/\text{SLAO}(001)$ system if we consider the reconstructed interface geometry observed in TEM. These changes are not only quantitative, but also qualitative, as they are driven by considerably increased intraorbital $3d_{z^2}$

scattering and further promoted by contributions from the interorbital $3d_{x^2-y^2}$ - $3d_{z^2}$ channel (Fig. 4, bottom row). Both clearly surpass the $3d_{x^2-y^2}$ channel.

We identify that this phenomenon originates predominantly from the emergent Ni $3d_{z^2}$ states localized near the interface, which contribute strongly to the density of states at the Fermi level and exhibit favorable Fermi surface nesting properties (Figs. 1 and 2). Together, these effects result in the strong amplification of the spin fluctuations. Considering that recent experiments reporting ambient-pressure superconductivity in strained systems are performed on capped bilayer nickelate films of 4 to 6 bilayers thickness [53–55], these findings suggest that interfacial effects may play a key role in the emergence of superconductivity in La₃Ni₂O₇ on SLAO(001).

III. DISCUSSION

We investigated the effect of compressive strain and interface reconstructions in La₃Ni₂O₇ on SrLaAlO₄(001) by performing first-principles simulations including a Coulomb repulsion term, treating the interface explicitly.

Comparison of the structural optimization results, specifically the evolution of the vertical lattice parameter of the bilayer nickelate on different technologically relevant substrates, with recent x-ray diffraction and transmission electron microscopy measurements on strained epitaxial thin films revealed close agreement and highlighted the key role of the reconstructed interface composition. We observed finite octahedral tilts throughout the bilayer nickelate. Intriguingly, these tilts are suppressed at the reconstructed interface, accompanied by significantly enhanced spin fluctuations. This finding provides an important contribution to the ongoing debate on whether superconductivity in bilayer nickelates requires a structural transition to the high-symmetry I4/mmm phase or can arise from purely electronic effects [24, 50].

We found that compressive strain drives an electronic reconstruction in the bilayer nickelate, characterized by an unconventional occupation of the antibonding Ni $3d_{z^2}$ states with simultaneous absence of interfacial charge transfer. This scenario contrasts sharply with the notion of metallized bonding Ni $3d_{z^2}$ states, considered to be critical for the superconducting state in pressurized bulk La₃Ni₂O₇. The concomitant substantial modifications of the Fermi surface and amplified spin fluctuations, especially for the reconstructed interface due to the emergent Ni $3d_{z^2}$ states, point to an electron pairing that deviates fundamentally from the flat-band physics dominant under hydrostatic pressure.

The pronounced influence of epitaxial strain and interface effects underscores the potential of strain and interface engineering to tailor the electronic structure and optimize the superconducting properties in bilayer nickelates at ambient pressure, circumventing the challenges associated with high-pressure synthesis and characterization and offering a pathway towards realizing their full technological potential.

ACKNOWLEDGMENTS

This work was supported by the National Science Foundation, Grant No. NSF-DMR-2118718.

IV. METHODS

A. Density functional theory calculations

We performed first-principles calculations in the framework of density functional theory [62] (DFT) as implemented in the Quantum Espresso code [63]. The generalized gradient approximation was used for the exchange and correlation functional as parametrized by Perdew, Burke, and Ernzerhof [64] in conjunction with ultrasoft pseudopotentials [65], as successfully employed in previous work [61, 66, 67]. Static correlation effects were considered within the DFT+U formalism [68], employing U = 4 eV on the Ni and Ti 3dstates [1, 16, 50, 69-71]. Octahedral rotations are fully accounted for by using $\sqrt{2}a \times \sqrt{2}a \times c$ supercells with two transition metal sites per layer, setting a to the substrate lattice parameter of $a_{SLAO} = 3.756 \text{ Å } [53, 57]$ and accurately optimizing c as well as the ionic positions. The symmetric supercells contain two equivalent interfaces, 3 bilayers of La₃Ni₂O₇, and 5 layers of substrate, corresponding to 142 atoms (Fig. 1). Wave functions and density were expanded into plane waves up to cutoff energies of 35 and 350 Ry, respectively. The Brillouin zone was sampled by using a $12 \times 12 \times 1$ Monkhorst-Pack \vec{k} -point grid [72] and 5 mRy Methfessel-Paxton smearing [73]. The ionic positions were accurately optimized, reducing ionic forces below 1 mRy/a.u. Subsequently, Fermi surfaces and densities of states were obtained by using $64 \times 64 \times 4$ \vec{k} -point grids. Reference calculations for ambient-pressure bulk La₃Ni₂O₇ (Cmcm) were performed by using 48-atom supercells [24, 34] with $12 \times 12 \times 4$ and $64 \times 64 \times 8$ \vec{k} -point grids.

B. Tight-binding Hamiltonians in a basis of maximally localized Wannier functions

We constructed tight-binding Hamiltonians describing the physics of the Ni e_g states, which are the active states near the Fermi level, in a basis of maximally localized Wannier functions for all bilayer nickelate systems considered in this work. The tight-binding models describe 12 (8) distinct Ni sites and thus 24 (16) Ni orbitals for the system with ideal (reconstructed) interface, which can be further reduced by exploiting symmetries. The output files of wannier90 [74], which can be directly imported into different post-processing programs, are conveniently provided at https://github.com/henniggroup.

C. Spin susceptibility calculations

Using these tight-binding Hamiltonians, we computed the bare generalized susceptibility $\chi^{(0)}_{abcd}(\mathbf{q})$ at $T=60~\mathrm{K}$ ($\beta=200$) leveraging the Toolbox for Research on Interacting Quantum Systems-Two-Particle Response Function (TRIQS-TPRF) framework [75] by Fourier transform of

$$\chi_{abcd}^{(0)}(\mathbf{r}) = -\int_0^\beta d\tau \, G_{da}^{(0)}(\tau, \mathbf{r}) G_{bc}^{(0)}(-\tau, -\mathbf{r})$$

from non-interacting single-particle Green's functions defined on a mesh of Matsubara frequencies

$$G_{ab}^{(0)}(\mathbf{k}, i\omega_n) = [i\omega_n \cdot \mathbf{1} - \epsilon(\mathbf{k})]^{-1}$$
,

where $\epsilon_{ab}(\mathbf{k})$ is the matrix-valued dispersion relation. The indices label the different orbitals $(3d_{z^2}$ and $3d_{x^2-y^2})$ at the different Ni sites. Note that we employ the full tight-binding Hamiltonian based on the $\sqrt{2} \times \sqrt{2}$ supercell here instead of a simplified model, describing *explicitly* all Ni sites to accurately treat effects of octahedral rotations and electrostatic doping. Subsequently, we consider a Kanamori-type interaction vertex during the calculation of $\chi^{\text{RPA}}_{abcd}(\mathbf{q})$ in the random

phase approximation (RPA),

$$\chi^{\text{RPA}}(\mathbf{q}) = \left(1 - \chi^{(0)}(\mathbf{q}) \, \Gamma\right)^{-1} \chi^{(0)}(\mathbf{q})$$

with

$$\Gamma_{abcd} = \begin{cases} U & \text{if } a = b = c = d \\ U' & \text{if } a = c \neq b = d \\ J & \text{if } a = b \neq c = d \\ J' & \text{if } a = d \neq b = c \\ 0 & \text{else} \end{cases}$$

where U'=U-2J and J'=J. Notably, Γ_{abcd} characterizes electronic correlations involving orbitals at the same Ni site, vanishing if any indices correspond to distinct sites. Finally, we implemented a strategy to unfold the result from the $\sqrt{2} \times \sqrt{2}$ to the full Brillouin zone by including structural phase factors and computed the 'physical' susceptibility by evaluating the trace:

$$\chi^{\text{RPA}}(\mathbf{q}) = \frac{1}{2} \sum_{a,b} \chi^{\text{RPA}}_{aabb}(\mathbf{q}) .$$

Leveraging this methodology, we are able to fully consider the effects of octahedral rotations and electrostatic doping that necessitate the use of large supercells, while displaying $\chi^{\text{RPA}}(\mathbf{q})$ without backfolding for direct comparison with future experiments.

- [1] H. Sun, M. Huo, X. Hu, J. Li, Z. Liu, Y. Han, L. Tang, Z. Mao, P. Yang, B. Wang, J. Cheng, D.-X. Yao, G.-M. Zhang, and M. Wang, Signatures of superconductivity near 80 K in a nickelate under high pressure, Nature 621, 493 (2023).
- [2] J. Hou, P.-T. Yang, Z.-Y. Liu, J.-Y. Li, P.-F. Shan, L. Ma, G. Wang, N.-N. Wang, H.-Z. Guo, J.-P. Sun, Y. Uwatoko, M. Wang, G.-M. Zhang, B.-S. Wang, and J.-G. Cheng, Emergence of high-temperature superconducting phase in pressurized La₃Ni₂O₇ crystals, Chin. Phys. Lett. 40, 117302 (2023).
- [3] Y. Zhang, D. Su, Y. Huang, Z. Shan, H. Sun, M. Huo, K. Ye, J. Zhang, Z. Yang, Y. Xu, Y. Su, R. Li, M. Smidman, M. Wang, L. Jiao, and H. Yuan, High-temperature superconductivity with zero resistance and strange-metal behaviour in La₃Ni₂O_{7-δ}, Nature Physics 20, 1269 (2024).
- [4] Z. Luo, X. Hu, M. Wang, W. Wú, and D.-X. Yao, Bilayer twoorbital model of La₃Ni₂O₇ under pressure, Phys. Rev. Lett. 131, 126001 (2023).
- [5] Y. Gu, C. Le, Z. Yang, X. Wu, and J. Hu, Effective model and pairing tendency in bilayer Ni-based superconductor La₃Ni₂O₇ (2023), arXiv:2306.07275 [cond-mat.supr-con].
- [6] Q.-G. Yang, D. Wang, and Q.-H. Wang, Possible s_±-wave superconductivity in La₃Ni₂O₇, Phys. Rev. B 108, L140505 (2023).
- [7] F. Lechermann, J. Gondolf, S. Bötzel, and I. M. Eremin, Electronic correlations and superconducting instability in La₃Ni₂O₇ under high pressure, Phys. Rev. B 108, L201121 (2023).

- [8] H. Sakakibara, N. Kitamine, M. Ochi, and K. Kuroki, Possible high T_c superconductivity in La₃Ni₂O₇ under high pressure through manifestation of a nearly half-filled bilayer Hubbard model, Phys. Rev. Lett. **132**, 106002 (2024).
- [9] Y. Shen, M. Qin, and G.-M. Zhang, Effective bi-layer model hamiltonian and density-matrix renormalization group study for the high- T_c superconductivity in La₃Ni₂O₇ under high pressure, Chin. Phys. Lett. **40**, 127401 (2023).
- [10] V. Christiansson, F. Petocchi, and P. Werner, Correlated electronic structure of La₃Ni₂O₇ under pressure, Phys. Rev. Lett. 131, 206501 (2023).
- [11] D. A. Shilenko and I. V. Leonov, Correlated electronic structure, orbital-selective behavior, and magnetic correlations in doublelayer La₃Ni₂O₇ under pressure, Phys. Rev. B 108, 125105 (2023)
- [12] W. Wú, Z. Luo, D.-X. Yao, and M. Wang, Superexchange and charge transfer in the nickelate superconductor La₃Ni₂O₇ under pressure, Science China Physics, Mechanics & Astronomy 67, 117402 (2024).
- [13] Y. Cao and Y.-f. Yang, Flat bands promoted by Hund's rule coupling in the candidate double-layer high-temperature superconductor La₃Ni₂O₇ under high pressure, Phys. Rev. B 109, L081105 (2024).
- [14] X. Chen, P. Jiang, J. Li, Z. Zhong, and Y. Lu, Critical charge and spin instabilities in superconducting La₃Ni₂O₇ (2023), arXiv:2307.07154 [cond-mat.supr-con].

- [15] C. Lu, Z. Pan, F. Yang, and C. Wu, Interlayer-coupling-driven high-temperature superconductivity in La₃Ni₂O₇ under pressure, Phys. Rev. Lett. 132, 146002 (2024).
- [16] Y. Zhang, L.-F. Lin, A. Moreo, T. A. Maier, and E. Dagotto, Structural phase transition, s±-wave pairing, and magnetic stripe order in bilayered superconductor La₃Ni₂O₇ under pressure, Nat. Commun. 15, 2470 (2024).
- [17] Z. Liao, L. Chen, G. Duan, Y. Wang, C. Liu, R. Yu, and Q. Si, Electron correlations and superconductivity in La₃Ni₂O₇ under pressure tuning (2023), arXiv:2307.16697 [cond-mat.suprconl.
- [18] X.-Z. Qu, D.-W. Qu, J. Chen, C. Wu, F. Yang, W. Li, and G. Su, Bilayer t-j-j⊥ model and magnetically mediated pairing in the pressurized nickelate La₃Ni₂O₇, Phys. Rev. Lett. 132, 036502 (2024).
- [19] J. Huang, Z. D. Wang, and T. Zhou, Impurity and vortex states in the bilayer high-temperature superconductor La₃Ni₂O₇, Phys. Rev. B 108, 174501 (2023).
- [20] Q. Qin and Y.-f. Yang, High- T_c superconductivity by mobilizing local spin singlets and possible route to higher T_c in pressurized La₃Ni₂O₇, Phys. Rev. B **108**, L140504 (2023).
- [21] Y.-B. Liu, J.-W. Mei, F. Ye, W.-Q. Chen, and F. Yang, s^{\pm} -wave pairing and the destructive role of apical-oxygen deficiencies in La₃Ni₂O₇ under pressure, Phys. Rev. Lett. **131**, 236002 (2023).
- [22] Y. Zhang, L.-F. Lin, A. Moreo, T. A. Maier, and E. Dagotto, Trends in electronic structures and s_{\pm} -wave pairing for the rare-earth series in bilayer nickelate superconductor $R_3 \text{Ni}_2 \text{O}_7$, Phys. Rev. B **108**, 165141 (2023).
- [23] Z. Liu, M. Huo, J. Li, Q. Li, Y. Liu, Y. Dai, X. Zhou, J. Hao, Y. Lu, M. Wang, and H.-H. Wen, Electronic correlations and partial gap in the bilayer nickelate La₃Ni₂O₇, Nat. Commun. 15, 7570 (2024).
- [24] B. Geisler, J. J. Hamlin, G. R. Stewart, R. G. Hennig, and P. J. Hirschfeld, Structural transitions, octahedral rotations, and electronic properties of A₃Ni₂O₇ rare-earth nickelates under high pressure, npj Quantum Materials 9, 38 (2024).
- [25] L. C. Rhodes and P. Wahl, Structural routes to stabilize superconducting La₃Ni₂O₇ at ambient pressure, Phys. Rev. Mater. 8, 044801 (2024).
- [26] G. Wang, N. Wang, J. Hou, L. Ma, L. Shi, Z. Ren, Y. Gu, X. Shen, H. Ma, P. Yang, Z. Liu, H. Guo, J. Sun, G. Zhang, J. Yan, B. Wang, Y. Uwatoko, and J. Cheng, Pressure-induced superconductivity in polycrystalline La₃Ni₂O₇ (2023), arXiv:2309.17378 [cond-mat.supr-con].
- [27] J. Yang, H. Sun, X. Hu, Y. Xie, T. Miao, H. Luo, H. Chen, B. Liang, W. Zhu, G. Qu, C.-Q. Chen, M. Huo, Y. Huang, S. Zhang, F. Zhang, F. Yang, Z. Wang, Q. Peng, H. Mao, G. Liu, Z. Xu, T. Qian, D.-X. Yao, M. Wang, L. Zhao, and X. J. Zhou, Orbital-dependent electron correlation in double-layer nickelate La₃Ni₂O₇ (2023), arXiv:2309.01148 [cond-mat.supr-con].
- [28] C. Lu, Z. Pan, F. Yang, and C. Wu, Interplay of two e_g orbitals in superconducting La₃Ni₂O₇ under pressure (2023), arXiv:2310.02915 [cond-mat.supr-con].
- [29] G. Wang, N. Wang, Y. Wang, L. Shi, X. Shen, J. Hou, H. Ma, P. Yang, Z. Liu, H. Zhang, X. Dong, J. Sun, B. Wang, K. Jiang, J. Hu, Y. Uwatoko, and J. Cheng, Observation of high-temperature superconductivity in the high-pressure tetragonal phase of La₂PrNi₂O_{7-δ} (2023), arXiv:2311.08212 [condmat.supr-con].
- [30] L. Wang, Y. Li, S. Xie, F. Liu, H. Sun, C. Huang, Y. Gao, T. Nakagawa, B. Fu, B. Dong, Z. Cao, R. Yu, S. I. Kawaguchi, H. Kadobayashi, M. Wang, C. Jin, H. kwang Mao, and H. Liu, Structure responsible for the superconducting state in

- La₃Ni₂O₇ at high pressure and low temperature conditions (2023), arXiv:2311.09186 [cond-mat.supr-con].
- [31] K. Chen, X. Liu, J. Jiao, M. Zou, C. Jiang, X. Li, Y. Luo, Q. Wu, N. Zhang, Y. Guo, and L. Shu, Evidence of spin density waves in La₃Ni₂O_{7-δ}, Phys. Rev. Lett. 132, 256503 (2024).
- [32] Y.-Y. Zheng and W. Wu, Superconductivity in the bilayer twoorbital hubbard model (2023), arXiv:2312.03605 [cond-mat.strel].
- [33] M. Kakoi, T. Kaneko, H. Sakakibara, M. Ochi, and K. Kuroki, Pair correlations of the hybridized orbitals in a ladder model for the bilayer nickelate La₃Ni₂O₇ (2023), arXiv:2312.04304 [cond-mat.supr-con].
- [34] B. Geisler, L. Fanfarillo, J. J. Hamlin, G. R. Stewart, R. G. Hennig, and P. J. Hirschfeld, Optical properties and electronic correlations in La₃Ni₂O₇ bilayer nickelates under high pressure, npj Quantum Materials 9, 89 (2024).
- [35] Z. Dong, M. Huo, J. Li, J. Li, P. Li, H. Sun, L. Gu, Y. Lu, M. Wang, Y. Wang, and Z. Chen, Visualization of oxygen vacancies and self-doped ligand holes in La₃Ni₂O_{7-δ}, Nature 630, 847 (2024).
- [36] X. Chen, J. Zhang, A. S. Thind, S. Sharma, H. LaBollita, G. Peterson, H. Zheng, D. P. Phelan, A. S. Botana, R. F. Klie, and J. F. Mitchell, Polymorphism in the ruddlesden–popper nickelate La₃Ni₂O₇: Discovery of a hidden phase with distinctive layer stacking, J. Am. Chem. Soc. 146, 3640 (2024).
- [37] N. Wang, G. Wang, X. Shen, J. Hou, J. Luo, X. Ma, H. Yang, L. Shi, J. Dou, J. Feng, J. Yang, Y. Shi, Z. Ren, H. Ma, P. Yang, Z. Liu, Y. Liu, H. Zhang, X. Dong, Y. Wang, K. Jiang, J. Hu, S. Nagasaki, K. Kitagawa, S. Calder, J. Yan, J. Sun, B. Wang, R. Zhou, Y. Uwatoko, and J. Cheng, Bulk high-temperature superconductivity in pressurized tetragonal La₂PrNi₂O₇, Nature 634, 579 (2024).
- [38] H. LaBollita, V. Pardo, M. R. Norman, and A. S. Botana, Assessing the formation of spin and charge stripes in La₃Ni₂O₇ from first-principles (2024), arXiv:2407.14409 [cond-mat.strell.
- [39] Z. Huo, Z. Luo, P. Zhang, A. Yang, Z. Liu, X. Tao, Z. Zhang, S. Guo, Q. Jiang, W. Chen, D.-X. Yao, D. Duan, and T. Cui, Modulation of the octahedral structure and potential superconductivity of La₃Ni₂O₇ through strain engineering, Science China Physics, Mechanics and Astronomy 68, 237411 (2025).
- [40] D. Li, K. Lee, B. Y. Wang, M. Osada, S. Crossley, H. R. Lee, Y. Cui, Y. Hikita, and H. Y. Hwang, Superconductivity in an infinite-layer nickelate, Nature 572, 624 (2019).
- [41] Q. Li, C. He, J. Si, X. Zhu, Y. Zhang, and H.-H. Wen, Absence of superconductivity in bulk Nd_{1-x}Sr_xNiO₂, Communications Materials 1, 16 (2020).
- [42] A. S. Botana and M. R. Norman, Similarities and differences between LaNiO₂ and CaCuO₂ and implications for superconductivity, Phys. Rev. X 10, 011024 (2020).
- [43] D. Li, B. Y. Wang, K. Lee, S. P. Harvey, M. Osada, B. H. Goodge, L. F. Kourkoutis, and H. Y. Hwang, Superconducting dome in $Nd_{1-x}Sr_xNiO_2$ infinite layer films, Phys. Rev. Lett. **125**, 027001 (2020).
- [44] S. Zeng, C. S. Tang, X. Yin, C. Li, M. Li, Z. Huang, J. Hu, W. Liu, G. J. Omar, H. Jani, Z. S. Lim, K. Han, D. Wan, P. Yang, S. J. Pennycook, A. T. S. Wee, and A. Ariando, Phase diagram and superconducting dome of infinite-layer Nd_{1-x}Sr_xNiO₂ thin films, Phys. Rev. Lett. 125, 147003 (2020).
- [45] M. Osada, B. Y. Wang, B. H. Goodge, K. Lee, H. Yoon, K. Sakuma, D. Li, M. Miura, L. F. Kourkoutis, and H. Y. Hwang, A superconducting praseodymium nickelate with infinite layer structure, Nano Lett. 20, 5735 (2020).

- [46] B.-X. Wang, H. Zheng, E. Krivyakina, O. Chmaissem, P. P. Lopes, J. W. Lynn, L. C. Gallington, Y. Ren, S. Rosenkranz, J. F. Mitchell, and D. Phelan, Synthesis and characterization of bulk Nd_{1-x}Sr_xNiO₂ and Nd_{1-x}Sr_xNiO₃, Phys. Rev. Materials 4, 084409 (2020).
- [47] M. Osada, B. Y. Wang, B. H. Goodge, S. P. Harvey, K. Lee, D. Li, L. F. Kourkoutis, and H. Y. Hwang, Nickelate superconductivity without rare-earth magnetism: (La,Sr)NiO₂, Adv. Mater. 33, 2104083 (2021).
- [48] B. H. Goodge, B. Geisler, K. Lee, M. Osada, B. Y. Wang, D. Li, H. Y. Hwang, R. Pentcheva, and L. F. Kourkoutis, Resolving the polar interface of infinite-layer nickelate thin films, Nat. Mater. 22, 466 (2023).
- [49] C. Xia, H. Liu, S. Zhou, and H. Chen, Sensitive dependence of pairing symmetry on Ni-e_g crystal field splitting in the nickelate superconductor La₃Ni₂O₇, Nat. Commun. 16, 1054 (2025).
- [50] B. Geisler, J. J. Hamlin, G. R. Stewart, R. G. Hennig, and P. J. Hirschfeld, Fermi surface reconstruction and enhanced spin fluctuations in strained La₃Ni₂O₇ on LaAlO₃(001) and SrTiO₃(001) (2024), arXiv:2411.14600 [cond-mat.supr-con].
- [51] Y.-F. Zhao and A. S. Botana, Electronic structure of Ruddlesden-Popper nickelates: strain to mimic the effects pressure (2024), arXiv:2412.04391 [cond-mat.supr-con].
- [52] H. C. R. B. Bhatta, X. Zhang, Y. Zhong, and C. Jia, Structural and electronic evolution of bilayer nickelates under biaxial strain (2025), arXiv:2502.01624 [cond-mat.supr-con].
- [53] E. K. Ko, Y. Yu, Y. Liu, L. Bhatt, J. Li, V. Thampy, C.-T. Kuo, B. Y. Wang, Y. Lee, K. Lee, J.-S. Lee, B. H. Goodge, D. A. Muller, and H. Y. Hwang, Signatures of ambient pressure superconductivity in thin film La₃Ni₂O₇, Nature 638, 935 (2025).
- [54] Y. Liu, E. K. Ko, Y. Tarn, L. Bhatt, B. H. Goodge, D. A. Muller, S. Raghu, Y. Yu, and H. Y. Hwang, Superconductivity and normal-state transport in compressively strained La₂PrNi₂O₇ thin films (2025), arXiv:2501.08022 [cond-mat.supr-con].
- [55] G. Zhou, W. Lv, H. Wang, Z. Nie, Y. Chen, Y. Li, H. Huang, W. Chen, Y. Sun, Q.-K. Xue, and Z. Chen, Ambient-pressure superconductivity onset above 40 K in (La,Pr)₃Ni₂O₇ films, Nature 10.1038/s41586-025-08755-z (2025).
- [56] T. Cui, S. Choi, T. Lin, C. Liu, G. Wang, N. Wang, S. Chen, H. Hong, D. Rong, Q. Wang, Q. Jin, J.-O. Wang, L. Gu, C. Ge, C. Wang, J.-G. Cheng, Q. Zhang, L. Si, K.-j. Jin, and E.-J. Guo, Strain-mediated phase crossover in Ruddlesden–Popper nickelates, Communications Materials 5, 32 (2024).
- [57] L. Bhatt, A. Y. Jiang, E. K. Ko, N. Schnitzer, G. A. Pan, D. F. Segedin, Y. Liu, Y. Yu, Y.-F. Zhao, E. A. Morales, C. M. Brooks, A. S. Botana, H. Y. Hwang, J. A. Mundy, D. A. Muller, and B. H. Goodge, Resolving structural origins for superconductivity in strain-engineered La₃Ni₂O₇ thin films (2025), arXiv:2501.08204 [cond-mat.supr-con].
- [58] J. Chaloupka and G. Khaliullin, Orbital order and possible superconductivity in LaNiO₃/LaMO₃ superlattices, Phys. Rev. Lett. 100, 016404 (2008).
- [59] P. Hansmann, X. Yang, A. Toschi, G. Khaliullin, O. K. Andersen, and K. Held, Turning a nickelate Fermi surface into a cupratelike one through heterostructuring, Phys. Rev. Lett. 103, 016401 (2009).
- [60] Z. Zhang, M. Greenblatt, and J. Goodenough, Synthesis, structure, and properties of the layered perovskite $La_3Ni_2O_{7-\delta}$, J. Solid State Chem. **108**, 402 (1994).
- [61] B. Geisler and R. Pentcheva, Inducing *n* and *p*-type thermoelectricity in oxide superlattices by strain tuning of orbital-

- selective transport resonances, Phys. Rev. Applied **11**, 044047 (2019).
- [62] W. Kohn and L. J. Sham, Self-consistent equations including exchange and correlation effects, Phys. Rev. 140, A1133 (1965).
- [63] P. Giannozzi, S. Baroni, N. Bonini, M. Calandra, R. Car, C. Cavazzoni, D. Ceresoli, G. L. Chiarotti, M. Cococcioni, I. Dabo, A. Dal Corso, S. de Gironcoli, S. Fabris, G. Fratesi, R. Gebauer, U. Gerstmann, C. Gougoussis, A. Kokalj, M. Lazzeri, L. Martin-Samos, N. Marzari, F. Mauri, R. Mazzarello, S. Paolini, A. Pasquarello, L. Paulatto, C. Sbraccia, S. Scandolo, G. Sclauzero, A. P. Seitsonen, A. Smogunov, P. Umari, and R. M. Wentzcovitch, QUANTUM ESPRESSO: a modular and open-source software project for quantum simulations of materials, J. Phys.: Condens. Matter 21, 395502 (2009).
- [64] J. P. Perdew, K. Burke, and M. Ernzerhof, Generalized gradient approximation made simple, Phys. Rev. Lett. 77, 3865 (1996).
- [65] D. Vanderbilt, Soft self-consistent pseudopotentials in a generalized eigenvalue formalism, Phys. Rev. B 41, 7892 (1990).
- [66] B. Geisler and R. Pentcheva, Confinement- and strain-induced enhancement of thermoelectric properties in LaNiO₃/LaAlO₃(001) superlattices, Phys. Rev. Materials 2, 055403 (2018).
- [67] F. Wrobel, B. Geisler, Y. Wang, G. Christiani, G. Logvenov, M. Bluschke, E. Schierle, P. A. van Aken, B. Keimer, R. Pentcheva, and E. Benckiser, Digital modulation of the nickel valence state in a cuprate-nickelate heterostructure, Phys. Rev. Materials 2, 035001 (2018).
- [68] M. Cococcioni and S. de Gironcoli, Linear response approach to the calculation of the effective interaction parameters in the LDA+U method, Phys. Rev. B 71, 035105 (2005).
- [69] B. Geisler and R. Pentcheva, Fundamental difference in the electronic reconstruction of infinite-layer versus perovskite neodymium nickelate films on SrTiO₃(001), Phys. Rev. B 102, 020502(R) (2020).
- [70] B. Geisler and R. Pentcheva, Correlated interface electron gas in infinite-layer nickelate versus cuprate films on SrTiO₃(001), Phys. Rev. Research 3, 013261 (2021).
- [71] B. Geisler, S. Follmann, and R. Pentcheva, Oxygen vacancy formation and electronic reconstruction in strained LaNiO₃ and LaNiO₃/LaAlO₃ superlattices, Phys. Rev. B 106, 155139 (2022).
- [72] H. J. Monkhorst and J. D. Pack, Special points for Brillouinzone integrations, Phys. Rev. B 13, 5188 (1976).
- [73] M. Methfessel and A. T. Paxton, High-precision sampling for Brillouin-zone integration in metals, Phys. Rev. B 40, 3616 (1989).
- [74] G. Pizzi, V. Vitale, R. Arita, S. Blügel, F. Freimuth, G. Géranton, M. Gibertini, D. Gresch, C. Johnson, T. Koretsune, J. Ibanez-Azpiroz, H. Lee, J.-M. Lihm, D. Marchand, A. Marrazzo, Y. Mokrousov, J. I. Mustafa, Y. Nohara, Y. Nomura, L. Paulatto, S. Poncé, T. Ponweiser, J. Qiao, F. Thöle, S. S. Tsirkin, M. Wierzbowska, N. Marzari, D. Vanderbilt, I. Souza, A. A. Mostofi, and J. R. Yates, Wannier90 as a community code: new features and applications, J. Phys.: Condens. Matter 32, 165902 (2020).
- [75] O. Parcollet, M. Ferrero, T. Ayral, H. Hafermann, I. Krivenko, L. Messio, and P. Seth, TRIQS: A toolbox for research on interacting quantum systems, Computer Physics Communications 196, 398 (2015).